Three-dimensional Core@Shell Nano-Array Electrodes for Integrated Lithium-Ion Microbatteries

Y. Mao[*], X. Sun[*], Q. Li[*,**], and Y. Lü[***]

[*]Department of Chemistry, University of Texas - Pan American, Edinburg, TX 78539 USA, maoy@utpa.edu

[**]Department of Mechanical Engineering, University of Texas - Pan American, Edinburg, TX 78539 USA

[***]College of Materials Science and Engineering, Nanjing University of Technology, Nanjing 210009, China

ABSTRACT

To overcome the distinct challenge posed on the clumsy two-dimensional configuration that was originally designed and currently widely employed for electrochemical energy storage devices with large lateral dimension, here we designed and synthesized two types of electrochemical electrodes with three-dimensional (3D) configurations on titanium substrate. Structural characterization and electrochemical measurements on electrodes composed of the ZnO@MnO_2 core@shell nanowire arrays or nanoforests (*i.e.* branched nanowire arrays) demonstrated that the electrodes with novel nanoforest architecture possess better electrical conductivity, larger surface area, and higher electrochemically active material loading than their nanowire array counterparts. More specifically, the nanoforest electrodes exhibit five times higher areal capacitance, better rate performance, as well as smaller inner resistance than nanowire array electrodes. These novel 3D architectures offer promising designs for powering microelectronics and other small autonomous devices with exceptionally small geometric scales.

Keywords: core@shell; energy storage; manganese oxide; nanoforest; three-dimensional

INTRODUCTION

Supercapacitors and lithium ion batteries as two electrochemical energy storage devices have attracted increasing attention in recent years, owing to the high power density, excellent reversibility, long cycle life and good operational safety of the former and the high energy density of the latter.[1-3] However, their miniaturization has not kept pace with advances of microelectromechanical systems (MEMS), biomedical and autonomous devices, whose desired on-board power storage happens in exceptionally small geometric scales. In either unit weight (Wh/kg) or volume (Wh/L), the amount of energy stored on given footprint (J/mm^2) of these devices precedes that of conventional two-dimensional battery and supercapacitor configurations. To address the shortcomings of 2D battery and supercapacitor technology while developing more powerful electrodes,[4] one of the major approaches pursued very recently is based on the fabrication of three-dimensional (3D) electrode structure at nanoscale.[2, 5, 6]

Compared with compact two-dimensional (2D) counterparts, 3D architectures take advantage of the vertical dimension – height. 3D nanostructured electrodes possess higher surface/body ratios, larger surface areas, more surface active sites within a small footprint area, and accordingly enlarged areal capacity.[4, 7] Therefore, they are now considered as a new strategy for powering MEMS and other small autonomous devices.[4] Some efforts have been devoted to engineering 3D nanostructures as electrochemical energy storage electrodes. For examples, Liu *et al.* built electrodes made of Co_3O_4@MnO_2 nanowire arrays through sacrificial reactive 3D carbon template layers.[8] Xia *et al.* synthesized Co_3O_4@NiO core@shell nanowire arrays for supercapacitors with outstanding high capacitance and good cycling stability.[9] Yan *et al.* coated V_2O_5 on SnO_2 nanowire arrays to bridge the performance gap between batteries and supercapacitors for high-rate lithium ion batteries.[10] All these 3D core@shell heterostructures discussed here consist of high conductive 1D nanowires as the core and electroactive transition metal oxide/hydroxide as the shell. In this manuscript, inspired by branched trees with larger surface area to capture more sunlight,[11] we postulated that novel electrode architecture composed of branched nanowire arrays, i.e. forest of nanotrees, could possess further boosted electrochemical performance over that of 1D nanowire arrays. To our best knowledge, no electrodes composed of nanoforests have been applied to electrochemical energy storage devices yet.

More specifically, we first successful fabricated both 3D ZnO@MnO_2 core@shell nanowire arrays and their 3D branched nanowire array counterparts, *i.e.* nanoforests, using hydrothermal and redox processes in this study. Moreover, our electrochemical characterization revealed that 3D ZnO@MnO_2 core@shell nanoforest electrodes possess better rate performance, higher capacitance, and longer retention of capacitance at higher current densities, compared to their ZnO@MnO_2 core@shell nanowire array

counterparts. The main reasons behind the superior electrochemical performance of the nanoforest electrode possibly include: (i) more electroactive MnO_2 nanoparticles were coated onto the 3D ZnO backbone nanotrees with larger surface area than the nanowire arrays as the backbone with the same footprint; (ii) comparatively higher percentage of electroactive MnO_2 coating were deposited onto the ZnO branches than the ZnO trunk due to the smaller diameter of the former; and (iii) the extra loading of the coated electroactive MnO_2 nanoparticles on this novel 3D ZnO nanoforest architecture over that of nanowire array counterpart were also finely dispersed, directly grown on the current collector, and so still have fast charge transport paths.[4] Hence, this report fills the void in the gallery of heterostructured nanomaterials with 3D skeleton applied in energy storage. We also expect that the conceptual brilliance of the current study provides a direction to meet the miniaturization requirements of electrochemical power sources from MEMS and other miniaturized functional devices.

RESULTS AND DISCUSSION

Figure 1 shows SEM images of the 3D ZnO@MnO_2 core@shell nanowire arrays and nanoforests. These arrays have average lengths over 10 µm, grown perpendicularly on the substrate of titanium current collector (inset of Figure 1a). Figures 1a and 1b clearly present the nanowire arrays, and Figures 1c and 1d exhibit the typical morphology of the ZnO@MnO_2 nanotrees. Each of these nanotrees consists of 3D ZnO@MnO_2 nanowire as trunks and ZnO@MnO_2 nanorods on the trunks as branches with an average length of ~800 nm.

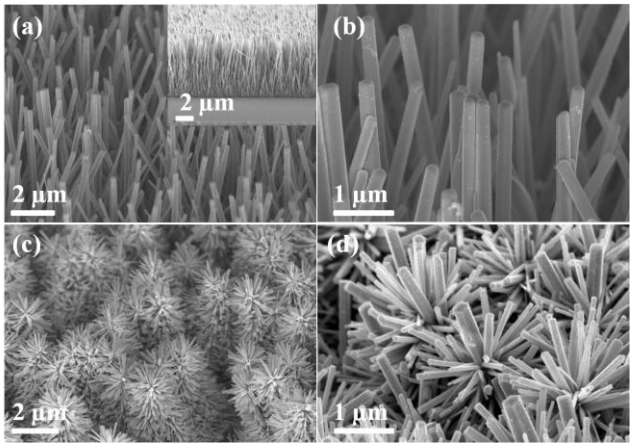

Figure 1. Typical SEM images of the synthesized 3D ZnO@MnO_2 core@shell (a & b) nanowire arrays and (c, d) branched nanowire arrays, i.e. forest of nanotrees. Reproduced by permission of The Royal Society of Chemistry: Chem. Commun., DOI: 10.1039/C3CC41048J.

Figure 2 exhibits (HR)TEM images of individual ZnO@MnO_2 core@shell nanowire and branched nanowie. These images clearly demonstrate that a well-dispersed MnO_2 nanoparticle layer with a thickness of ~3 nm was coated on the entire surface of the single crystalline ZnO nanowire backbone.

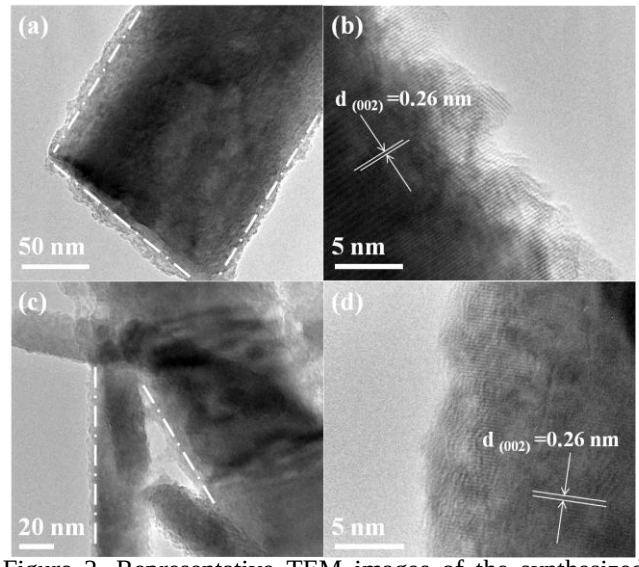

Figure 2. Representative TEM images of the synthesized 3D ZnO@MnO_2 core@shell (a and b) nanowire arrays and (c and d) nanoforests: (a) TEM image taken from the end of an individual nanowire; (b) HRTEM image focusing on the edge of an individual nanowire shown in (a); (c) TEM image taken from one part of an individual branched nanowire; (d) HRTEM image focusing on the edge of an individual branched nanowire shown in (c). Reproduced by permission of The Royal Society of Chemistry: Chem. Commun., DOI: 10.1039/C3CC41048J.

Cyclic voltammetry (CV) measurements (Figure 3a) were taken on the synthesized 3D ZnO@MnO_2 core@shell nanoforests as the working electrode in a three-electrode system at different scan rates of 2, 5, 10, 20, 50, and 100 mV/s. In the potential range of -0.2 to 0.6 V (vs Ag/AgCl), no obvious redox peaks were observed. This is characteristic to electroactive MnO_2 in this potential range. It indicates that electrodes made from our synthesized 3D ZnO@MnO_2 core@shell nanoforests can absorb cations (e.g. Na^+ and proton H_3O^+) onto its surface and/or subsurface from electrolyte:

$$MnO_2 + M^+ + e^- \leftrightarrow MnOOM,\ M^+ = Na^+ \text{ or } H_3O^+ \quad (1)$$

and experience possible intercalation or deintercalation of Na^+ or H_3O^+.[14] Moreover, these CV curves exhibit approximately rectangular shape, especially at slow scan rates. This observation indicates an excellent capacitive behavior and a low contact resistance of the electrodes made from our synthesized 3D ZnO@MnO_2 core@shell nanoforests, consistent with EIS data shown below. As commonly observed and expected, the rectangularity is gradually expanding and distorted with increasing scan rates. However, the CV curves taken at the same scan rates from electrodes made of the 3D ZnO@MnO_2 core@shell nanowire array counterpart are more evidently distorted and

possess much smaller area (data not shown). It suggests that the 3D ZnO@MnO_2 core@shell nanowire arrays possess faster downgrading capacitance than the nanoforests even though both 3D ZnO@MnO_2 core@shell nanoarchitectures are composed of the same materials (including core ZnO, shell MnO_2, and the current collector Ti substrate) and were fabricated by the same procedure. Furthermore, by comparing the CV curves taken at the scan rate of 2 mV/s of electrodes with same lateral size made from the 3D ZnO@MnO_2 core@shell nanoforests, their nanowire array counterpart and the pure titanium substrate (Figure 3b), a significant increase in integrated CV area was observed from the 3D ZnO@MnO_2 core@shell nanoforest electrode over the 3D ZnO@MnO_2 core@shell nanowire array electrode, while the pure titanium substrate shows barely any capacitance. The much larger capacitance of the 3D ZnO@MnO_2 core@shell nanoforest electrode can be attributed to the larger accessible surface area of its unique nanoarchitecture and higher loading of the electroactive MnO_2 nanoparticle coating over that of the 3D ZnO@MnO_2 core@shell nanowire array counterpart at the same footprint.

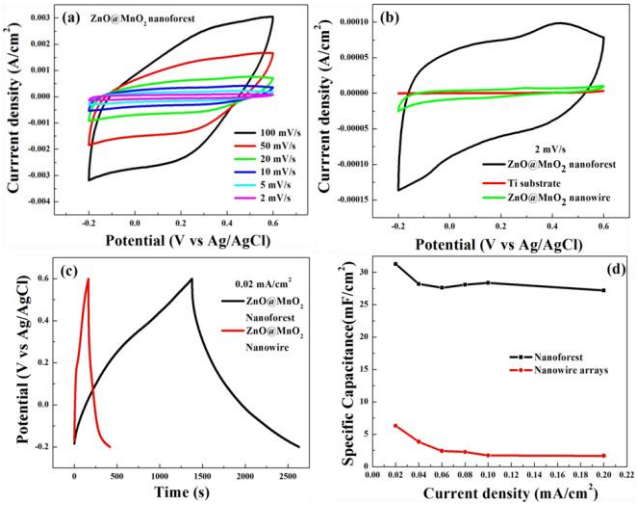

Figure 3. (a) Cyclic Voltammetry (CV) curves of the 3D ZnO@MnO_2 core@shell nanforest electrode at different scan rates. (b) CV curves of the 3D ZnO@MnO_2 core@shell nanoforests, 3D ZnO@MnO_2 core@shell nanowire arrays, and titanium substrate as working electrodes at 2 mV/s. (c) Charging/discharging (CD) curves of working electrodes made of the 3D ZnO@MnO_2 core@shell nanoforests and nanowire arrays at current density of 0.02 mA/cm^2. (d) Specific discharging capacitances at different current densities of electrodes made of the 3D ZnO@MnO_2 core@shell nanoforest and nanowire arrays. Reproduced by permission of The Royal Society of Chemistry: Chem. Commun., DOI: 10.1039/C3CC41048J.

From the charge/discharge (CD) measurements conducted on both the 3D ZnO@MnO_2 core@shell nanoforest and nanowire array electrodes (Figures 3c), their specific areal capacitances C_{area} at different current densities (Figure 3d) were calculated according to both the charge/discharge profiles. The respective charging/discharging times are nearly the same, indicating superior reversibility of charging and discharging reactions of the electrodes made from both the synthesized 3D ZnO@MnO_2 core@shell nanoarchitectures. The C_{area} of 3D ZnO@MnO_2 core@shell nanoforest electrodes is estimated to be 31.30 mF/cm^2, which is nearly 5 times of that of the 3D ZnO@MnO_2 core@shell nanowire array electrodes (6.30 mF/cm^2). The high C_{area} of the 3D ZnO@MnO_2 core@shell nanoforest electrodes results from their enhanced surface area and higher loading amount of MnO_2 nanoparticle coating on the 3D ZnO nanoforest backbone over those of the 3D ZnO@MnO_2 core@shell nanowire array counterpart. This novel nanoforest architecture makes the utilization of space more efficient even than the nanowire array counterpart, guarantees effective interfacial contact between electrolyte and electroactive MnO_2 thin layer, and offers greatly improved electron transfer pathways by the 3D ZnO nanoforest backbone to the current collector.

Moreover, from Figure 3d, it is evident that the 3D ZnO@MnO_2 core@shell nanoforest electrodes delivers much superior high-rate capacity than the 3D ZnO@MnO_2 core@shell nanowire array electrodes. The 3D ZnO@MnO_2 core@shell nanoforest electrodes possess 87% capacitance retention (from 31.299 mF/cm^2 to 27.191 mF/cm^2) while the 3D ZnO@MnO_2 core@shell nanowire array electrodes has only 26% from 6.304 mF/cm^2 to 1.670 mF/cm^2) when discharging current density increased from 0.02 mA/cm^2 to 0.2 mA/cm^2. The higher rate capability of the 3D ZnO@MnO_2 core@shell nanoforest electrodes may be attributed to the unique 3D interconnected nanoarchitecture with elevated conductivity from the 3D ZnO nanoforest backbone and larger specific surface area on the same footprint. These structural advantages promote the maintenance of good electrochemical stability under larger voltage range and also accelerate charge separation and transport.[15-17] As reported in the literature, the decrease of specific capacitance with increasing current density results from the internal resistance of electrodes.[18] Therefore, the higher capacitance retention at high current densities of the 3D ZnO@MnO_2 core@shell nanoforest electrodes suggests a lower internal resistance over the corresponding nanowire array electrodes, as confirmed by our EIS data shown below. It also indicates the 3D ZnO@MnO_2 core@shell nanoforest electrodes should possess good stability as electrochemical energy storage devices due to their 3D interconnection.[19]

Generally speaking, compared to the conventional 2D electrode configurations of traditional batteries and supercapacitors, and even the most recently engineered 3D nanostructured electrodes, e.g. the as-synthesized 3D ZnO@MnO_2 core@shell nanowire arrays demonstrated in this study, our smartly designed electrodes with the 3D ZnO@MnO_2 core@shell nanoforest architecture are able to

enhance the surface area and loading of electroactive MnO_2 on the same lateral footprint while the 3D ZnO nanotree backbone provides an ideal pathway for efficient charge transport. More specifically, based on our synthetic procedure, conductive ZnO branches were uniformly grown from the surface of the ZnO nanowire array trunks, and electroactive MnO_2 nanoparticles were coated evenly on the entire surface of these 3D ZnO nanotrees. This leads to largely enhanced loading of a thin layer of coarse but uniform electroactive MnO_2 nanoparticle coating, analogous to tree barks, covering on the entire surface of ZnO nanotrees as well as the nanowire arrays (SEM images shown in Figures 1b and 1d). More electrochemically active MnO_2 surface from the 3D ZnO@MnO_2 core@shell nanoforest than that from the corresponding nanowire arrays allows higher access interfacial area with electrolyte, promoting the surface electrochemical reactions as superior energy storage electrodes with high specific capacitance and high rate capability.

Moreover, the MnO_2 shell coating is amorphous, as confirmed by HRTEM (Figures 2b and 2d). Amorphous MnO_2 was reported to be more desirable for supercapacitor applications owing to its high surface area and low mass density, compared with crystalline MnO_2.[20, 21] The thin layer of amorphous MnO_2 enables fast and reversible faradic reaction by shortening ion diffusion path with large areal loading to achieve high specific capacitance while the 3D ZnO nanotree backbone with high specific area provides highly conductive channels to effective electron transport like "highways". With this novel 3D backbone design of branched nanowire arrays, electrolyte ions can fully get access to the pores of amorphous MnO_2 thin layer, reacting with electrons delivered on the ZnO "highway". The novel design contributes to the superior capacitance and rate capability of our fabricated 3D ZnO@MnO_2 core@shell nanoforests with reduced diffusion lengths of ions, highly accessible surface area and good electrical conductivity. Further studies are underway by integrating these novel 3D ZnO@MnO_2 core@shell nanoforest electrodes into lithium ion batteries and supercapacitors. This new design not only fills the void in the gallery of heterostructured nanomaterials with 3D skeleton applied in electrochemical energy storage devices, but also provides a direction to meet the miniaturization requirements of powering MEMS and other miniaturized functional devices.

CONCLUSIONS

In summary, smartly designed 3D ZnO@MnO_2 core@shell nanoforests have been successfully synthesized for electrochemical energy storage electrodes. In such hierarchical electrodes, thin layer of amorphous electroactive MnO_2 coating with high surface area enables fast and reversible redox reactions with electrolyte to further improve the specific capacitance and rate capacity, while conductive 3D ZnO nanotrees working as the template for MnO_2 coating and the backbone of electron transport channels. This novel architecture efficiently increases the accessible surface area of electroactive materials to electrolyte, loading amount of electroactive materials per unit substrate area, and electrical conductivity of the hybrid electrode. These 3D ZnO@MnO_2 core@shell nanoforest electrodes offer higher areal capacitances, advanced rate capability, and better charge/discharge stability, compared with their corresponding nanowire array counterpart. The present work indicates that our smartly designed 3D nanoforest electrodes possess a great promise in applications for miniaturized energy storage devices.

REFERENCES

1 H. Jiang, C. Li, T. Sun and J. Ma, *Chem. Commun*., 2012, **48**, 2606.
2 S. Xin, Y. G. Guo and L. J. Wan, *Acc. Chem. Res*., 2012, **45**, 1759
3 J. Jiang, Y. Li, J. Liu, X. Huang, C. Yuan and X. W. Lou, *Adv. Mater*., 2012, **24**, 5166.
4 T. S. Arthur, D. J. Bates, N. Cirigliano, D. C. Johnson, P. Malati, J. M. Mosby, E. Perre, M. T. Rawls, A. L. Prieto and B. Dunn, *MRS Bulletin*, 2011, **36**, 523.
5 L. Q. Mai, F. Yang, Y. L. Zhao, X. Xu, L. Xu and Y. Z. Luo, *Nat. Commun*., 2011, **2**, 381.
6 J. Liu, J. Jiang, C. Cheng, H. Li, J. Zhang, H. Gong and H. J. Fan, *Adv. Mater*., 2011, **23**, 2076.
7 X. Xia, J. Tu, Y. Zhang, X. Wang, C. Gu, X. Zhao and H. J. Fan, *ACS Nano*, 2012, **6**, 5531.
8 J. Yan, A. Sumboja, E. Khoo and P. S. Lee, *Adv. Mater*., 2011, **23**, 746.
9 S. H. Ko, D. Lee, H. W. Kang, K. H. Nam, J. Y. Yeo, S, J. Hong, C. P. Grigoropoulos and H. J. Sung, *Nano Lett*., 2011, **11**, 666.
10 J. Liu, J. Jiang, M. Bosman and H. J. Fan, *J. Mater. Chem*., 2012, **22**, 2419.
11 Z. Lei, F. Shi and L. Lu, *ACS Appl. Mater. Interfaces*, 2012, **4**, 1058.
12 G. Yu, L. Hu, N. Liu, H. Wang, M. Vosgueritchian, Y. Yang and Y. Cui, Z. Bao, *Nano Lett*., 2011, **11**, 4438.
13 X. Lu, G. Wang. T. Zhai, M. Yu, J. Gan, Y. Tong and Y. Li, *Nano Lett*., 2012, **12**, 1690.
14 H. T. Nguyen, F. Yao, M. R. Zamfir, C. Biswas, K. P. So, Y. H. Lee, S. M. Kim, S. N. Cha, J. M. Kim and D. Pribat, *Adv. Energy Mater*., 2011, **1**, 1154.
15 R. B. Rakhi, W. Chen, D. Cha and H. N. Alshareef, *Nano Lett*., 2012, **12**, 2559.
16 L. Bao, J. Zang and X. Li, *Nano Lett*., 2011, **11**, 1215.
17 J. G. Wang, Y. Yang, Z. H. Huang and F. Kang, *J. Mater. Chem*., 2012, **22**, 16943.